Surface Science 760 (2025) 122776

Contents lists available at ScienceDirect

Surface Science

journal homepage: www.elsevier.com/locate/susc

Phosphonic acid adsorption on α-Bi_2O_3 surfaces

A. Bocchini [a,*,1], S. Kollmann [b,1], U. Gerstmann [a], W.G. Schmidt [a], G. Grundmeier [b]

[a] Department Physik, Universität Paderborn, 33095 Paderborn, Germany
[b] Department Chemie, Universität Paderborn, 33095 Paderborn, Germany

ARTICLE INFO

Keywords:
Bi_2O_3
Surface analysis
Phosphonic acid
DFT
XPS
FTIR

ABSTRACT

In this joint experiment-theory work the adsorption of organophosphonic acids on α-Bi_2O_3 surfaces is studied by means of X-ray photoelectron spectroscopy (XPS), diffuse reflectance infrared Fourier transform spectroscopy (DRIFTS), as well as density functional theory (DFT). The present results demonstrate the formation of a full bidentate-bonded monolayer structure with an all-trans configuration of the aliphatic chains, whereby the evolution of the monolayer can be monitored via the shape of XPS spectra. Our results for the model oxide are a basis for the surface modification of oxide covered Bi with functional organophosphonic acids.

1. Introduction

Bismuth electrodes are valued in a very broad range of applications due to their interesting properties, such as low toxicity, high electrochemical stability, and unique electronic structure. Example applications include battery technology [1], photovoltaics [2] and fuel cells [3], where they lead to improvements in efficiency and stability, as well as seawater desalination. Here, nanocrystalline Bi-foam electrodes may serve as an efficient and high capacity Cl-storage electrode [4]. In addition, they are being used in electrochemical catalysis [5,6], electrochemical [7] and biomedical sensing [8] and heavy-metal detection [9]. Bismuth films are also being explored in photodetectors [10]. In general, the material is a sustainable, effective option across various fields, serving as an environmentally friendly alternative to mercury-based electrodes and enhancing performance in sensing, energy storage, catalysis, and more.

The electrodes' properties are strongly influenced by their surface chemistry [11–14]. Under ambient conditions the bismuth electrodes are characterized by the formation of an oxide film [15]. The initial stages of the oxidation have been modeled, e.g., in Refs. [16,17]. Bismuth surface-oxide films are typically polycrystalline, and multiphase: While BiO dominates for very thin films [18], thicker oxide films show components of elemental Bi, BiO as well as Bi_2O_3 [19]. Bulk Bi_2O_3 occurs in several phases, whereby the so-called α phase is the one dominating under ambient conditions. Similar to bulk Bi, also bismuth oxides show a series of properties [19,20], which make it interesting to various applications, e.g., as dielectrics [21] or for catalysis [22,23].

It has been shown that oxide removal and stabilization of bismuth films is possible outside a vacuum environment using a wet chemistry approach using the self-assembly of 1-dodecanethiol as passivating agent [24]. Organothiols are also reported to increase the functionality for electrochemical sensor technology [25]. Also electrochemical indicators based on cyclic voltammetry have shown the formation of self-assembled monolayers (SAMs) of alkyl thiols on bismuth electrodes, and revealed that the defect structure as well as the stability of the SAMs depend on the length of the alkyl thiols [26].

In the context of surface functionalization, organophosphonic acids are commonly applied for the analogue modification of oxide-coated alloys or single-crystalline oxides [27–29]. Their adsorption mechanisms on various oxide-terminated surfaces, e.g., aluminum, magnesium, or titanium, have been investigated in detail. For example, it was found that these organophosphonic acids spontaneously self-assemble on aluminum-oxide surfaces, but longer adsorption times are required to produce dense, ordered films [20]. In addition, several studies also investigated the adsorption, ordering and stability of organophosphonic acids on refractive alloys with the main alloying elements being aluminum, titanium and zinc [30–35]. Infrared spectroscopy was used to analyze the monolayer ordering and the interfacial binding mechanisms [36,37], while a bidentate bonding of phosphonate groups to surface metal ions is often reported as the main reason for chemisorption [38–40]. In addition, in particular for low coverages, tridentate configurations are found [41].

As far as we know, no attempts have been made yet to functionalize bismuth or bismuth-oxide surfaces with phosphonic acids. This would be highly desirable, however: In particular in case of self-organized layers, organophosphonic acids are significantly less sensitive to oxidation compared to organothiols. This motivates the present joint

* Corresponding author.
E-mail address: adriana.bocchini@upb.de (A. Bocchini).
[1] These authors contributed equally to this work.

https://doi.org/10.1016/j.susc.2025.122776
Received 18 November 2024; Received in revised form 16 April 2025; Accepted 7 May 2025
Available online 16 May 2025

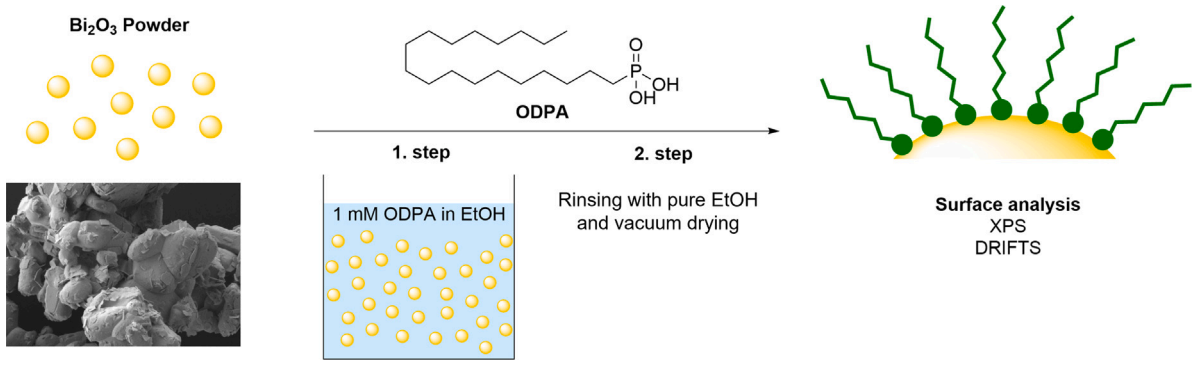

Fig. 1. Schematic representation of the surface modification of α-Bi_2O_3 powder with ODPA from an ethanolic solution. For details see main text.

experiment-theory study on the adsorption of phosphonates on α-Bi_2O_3 surfaces. By combining vibrational and electronic spectroscopy with density-functional-theory (DFT) calculations we explore the absorption of phosphonates on bismuth oxides in order to contribute to a knowledge-driven optimization of Bi coating procedures.

2. Methodology

2.1. Experiment

Bismuth-oxide powder (99.9%, Sigma Aldrich) with a mean particle size of 10 μm is used for the surface analytical studies. XRD powder studies were performed to determine the phase of the Bi_2O_3 particles [23]. For this investigation a Bruker D8 Advance diffractometer with a copper Kα radiation (40 kV, 40 mA) was used. The measurement was carried out in an angle range between 10° and 70° (2 theta) with a step size of 0.2° and a counting time of 3 s per step. The results of this measurement are shown in Fig. S2 in the Supplemental Materials and confirm that the particles are α-Bi_2O_3.

For surface functionalization, octadecyl phosphonic acid (ODPA) (97%, Sigma Aldrich) was dissolved in absolute (abs.) ethanol (Mundo oHG). More precisely, we added 5 g of Bi_2O_3 powder to 50 ml of ethanol, and mixed the suspension for two hours at room temperature on a vibrating plate. Afterwards, the so-modified powder was cleaned in abs. ethanol and dried using a rotary evaporator. This process is sketched in Fig. 1.

X-ray photoelectron spectroscopy (XPS) is performed using an Omicron ESCA+ system (Omicron NanoTechnology GmbH). This is equipped with an Al Kα (1486.3 eV) X-ray source. In addition, we use a hemispherical energy analyzer at a chamber pressure below $5 \cdot 10^{-10}$ mbar and a take-off angle of 60° with respect to the sample surface. Note that the measurements are carried out with neutralization. The filament current, the emission current as well as the beam energy amount to 1000 mA, 10 μA, and 1 eV, respectively. Survey spectra and the high-resolution core-level spectra are recorded with a pass energy of 100 eV and 20 eV, respectively. All the spectra are calibrated to the experimental C 1*s* peak (at 285.0 eV). For the data analysis we use the CasaXPS software (V2.3.23, Casa Software Ltd.). To evaluate the peak integrals, we use the corresponding relative sensitivity factor values. The background as well as the P 2*p* peak are fitted with a Shirley-type fit function. The signal peaks of the C 1*s*, O 1*s* and Bi 4*f* spectra are fitted with a Gaussian Lorentzian peak shape of 70% to 30%.

Diffuse reflectance infrared Fourier transform spectroscopy (DRIFTS) is carried out with a BrukerVertex70 (Bruker Optics, Germany) under dry air conditions. Thereby, a DTGS detector is employed, and the powders are filled in a funnel, which is provided for this purpose. In addition, KBr powder is used as the reference system. The resolution of the samples is 4 cm^{-1} and 512 scans are carried out. The OPUS software (V6.5 Bruker Optics GmbH) is used for evaluating the spectra.

2.2. Theory

Density-functional-theory (DFT) calculations are performed using the Quantum ESPRESSO (QE) package [42,43]. Norm-conserving pseudopotentials are used to model the electron-ion interaction. The electron exchange and correlation effects are described within the generalized gradient approximation (GGA), using the Perdew–Burke–Ernzerhof functional (PBE) [44]. The electron wave functions are expanded into plane waves up to a cutoff energy of 70 Ry. The Bi_2O_3(100) surface is modeled within a 320-atom supercell that contains a material slab composed of a 4 × 2 × 2-repeated α-Bi_2O_3 (monoclinic) unit cell [45–47], and about 20 Å of vacuum, see Fig. S4 in the Supplemental Materials. The surface termination is chosen following Ref. [48], i.e., using the energetically most favored $T_{2Bi(II)}$ model, which is stoichiometric and nonpolar [48].

The surface Brillouin zone is sampled using a 3 × 3 Monkhorst–Pack ***k***-point set [49]. Energy and force convergence criteria of 10^{-8} Ry and 10^{-4} Ry/bohr are employed for structural relaxation. The five central layers of the symmetric slab, see Fig. S4, are kept frozen at their ideal bulk positions. Methylphosphonic acid ($CH_3PO(OH)_2$, MPA) is used as model system to describe the adsorption of larger phosphonic acids by means of *first-principles* calculations. XPS spectra are simulated using a delta self-consistent field (ΔSCF) approach [50–53] which allows for the atomically resolved interpretation of the measured spectra [54]. Pseudopotentials with occupation-constrained inner shells were generated to model the core holes.

3. Surface characterization

3.1. Infrared spectroscopy

The DRIFTS analysis provides information on the binding mechanisms as well as the packing density of organic chains of ODPA. The survey spectrum is presented in Fig. 2 (a). The two insets shown in subfigures (b) and (c) correspond to the regions of the OH-stretching vibration and the phosphonate peak in the fingerprint region, respectively. Obviously, the ODPA adsorption leads to a decrease in the surface hydroxyl density (peak at 3720 cm^{-1}) and the adsorbed water layer thickness (broad peak at 3500 cm^{-1}).

In addition, in the fingerprint region in Fig. 2 (c) both the P=O peak and the phosphonate peak are present in the spectrum. The presence of the P=O peak hints at the presence of bidentate bonds. However, in parallel tridentate bonding might occur. The recent study of Schuschke et al. [41] shows that the binding modes might change with the surface coverage. For insolated adsorbed molecules a tridentate was found for a Co_3O_4(111) surface. However, with increasing surface coverage the bidentate binding mode became more dominant. Thus the parallel existence of both binding mechanism on the oxide powder is most likely. The respective peak assignments are compiled in Table 1. The DRIFTS analysis of ODPA adsorbed on Bi_2O_3 in comparison to ODPA mixed in

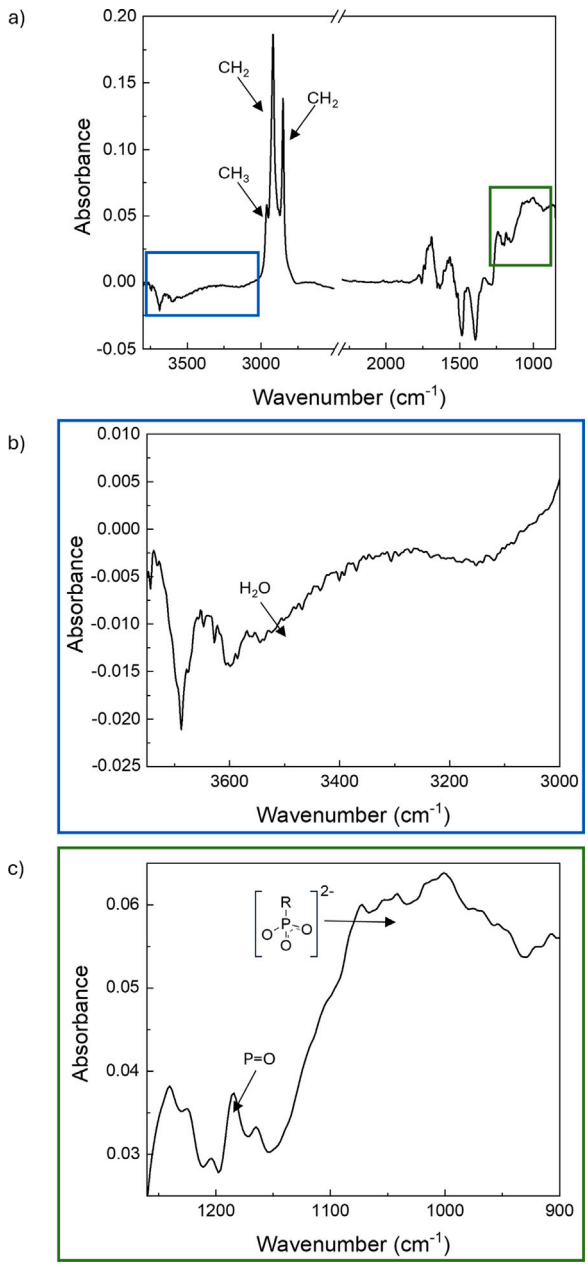

Fig. 2. DRIFTS analysis of the ODPA-modified α-Bi_2O_3 surface (a). The insets show region of the OH-stretching vibration (3000-3700 cm^{-1}) (b) and the fingerprint region with the peak of the phosphonate stretching (c).

Table 1
Peak assignments of the DRIFTS spectra based on literature.

Wavenumber	Vibration mode (cm^{-1})	Literature
3500	H_2O	Ref. [56]
2960	asym. CH_3	Ref. [39]
2918	asym. CH_2	Refs. [39,57]
2850	sym. CH_2	Refs. [39,57]
1631	H_2O	Ref. [56]
1185	P=O	Ref. [39,41]
1001 (1150–931)	PO_3^{2-}	Refs. [39,57]

KBr powder (see Fig. S1) shows a clear shift of the CH_2-stretching peak position to lower wavenumbers (2852 cm^{-1} to 2850 cm^{-1}). In agreement with Spori et al. [55], this peak shift indicates an all-trans configuration of the aliphatic chains of ODPA.

3.2. DFT models

To assist in the understanding of the adsorption mechanisms of phosphonic acids onto bismuth-oxide surfaces, we perform DFT total-energy calculations.

At first, stable hydroxyl-group terminated Bi_2O_3(100) surface structures are determined, starting from the bare, stoichiometric surface models suggested in Ref. [48]. We probed various coverages and structures and find that the arrangement in alternating chains of $BiO_4(OH)_2$-BiO_4 polyhedra along the [001] as shown in Fig. 3(a) is most favorable. Furthermore, we notice that shifting one of the $BiO_4(OH)_2$-BiO_4 chains by 1/4 of the lattice parameter along the [001] direction increases the energy by less than 150 meV. Thus, some disorder at the OH-terminated surface is possible, and this finding also suggests the possibility for the rearrangement of the hydroxyl groups in response to the adsorption of phosphonic acid.

The hydroxyl groups do not lead to a strong substrate relaxation, i.e., the OH-adsorbed surface resembles the structure of the bare surface. The hydroxylated surface features three differently coordinated bismuth atoms: There are Bi surface atoms that are either four- or six-fold coordinated to oxygen. Some of the six-fold coordinated Bi atoms experience a rather strong surface relaxation and are present already in case of the clean surface. In addition, there are the Bi atoms that remain in their bulk coordination, i.e., BiO_5. They may be subdivided into two groups with slightly different polyhedral volumes. Similarly, the O atoms can be divided into three groups: O atoms showing the bulk coordination, surface O atoms, and hydroxyl group O atoms.

To investigate the adsorption of phosphonic acids onto the bismuth oxide surface, we replace two of the hydroxyl groups on a $BiO_4(OH)_2$ polyhedron with one CH_3PO_3. Depending on the starting geometry, a number of equilibrium configurations is obtained. Two energetically relevant ones are depicted in Fig. 3 (b) and (c). For model A the MPA molecule adsorbs at two Bi surface atoms and it is almost perpendicular to the Bi_2O_3 surface. On the other hand, for model B, the PC bond forms an angle of about 25° with the surface, and the MPA molecule assumes a bidentate configuration. Thereby, model A is by about 180 meV more favorable compared to model B.

Upon the MPA absorption, the overall surface geometry remains almost unaffected. Nevertheless, the adsorbing Bi atoms are slightly shifted compared to their position in the fully hydroxylated surface. More precisely, for model A, the marked Bi atom is shifted by about 0.94 Å, while the second adsorbing Bi atom is risen by about 0.3 Å. For model B, on the other hand, the adsorbing Bi atom is lowered by about 0.3 Å compared to its previous position in the $BiO_4(OH)_2$ polyhedron. In addition, in both models, the phosphonic acid is distorted compared to its gas-phase structure: The $\overline{PC}$ bond length is enlarged by about 0.026 Å and 0.016 Å for model A and B, respectively, and also the angles formed by the central P atom with the O atom and the hydroxyl groups are affected to different extents.

In accordance with Ref. [41], for the investigation of denser coverages we study the simultaneous adsorption of two MPA molecules orientated as for model B, clearly showing a bidentate configuration. In addition, since our DRIFT analysis revealed an all-trans configuration, this finding is also reflected in our simulations. Here, six different configurations are possible, see Fig. 4. Depending on the configuration, the adsorption energy per molecule decreases by at least 73 meV. This shows a slightly repulsive interaction and suggests a rather uniform distribution of the adsorbed species. We find the molecules to be prone to adsorb on different polyhedral chains. However, the structures shown in Fig. 4 (c) and (d) are only slightly less favorable, suggesting some disorder in the overlayer formed. Generally, it is favorable for the molecules to adsorb in front of "empty" BiO_4 polyhedra, compare Fig. 4 (a) and (c) as well as (d) and (e). The configuration where two phosphonic acids adsorb on two adjacent BiO_4 polyhedra (Fig. 4 (f)) is not stable.

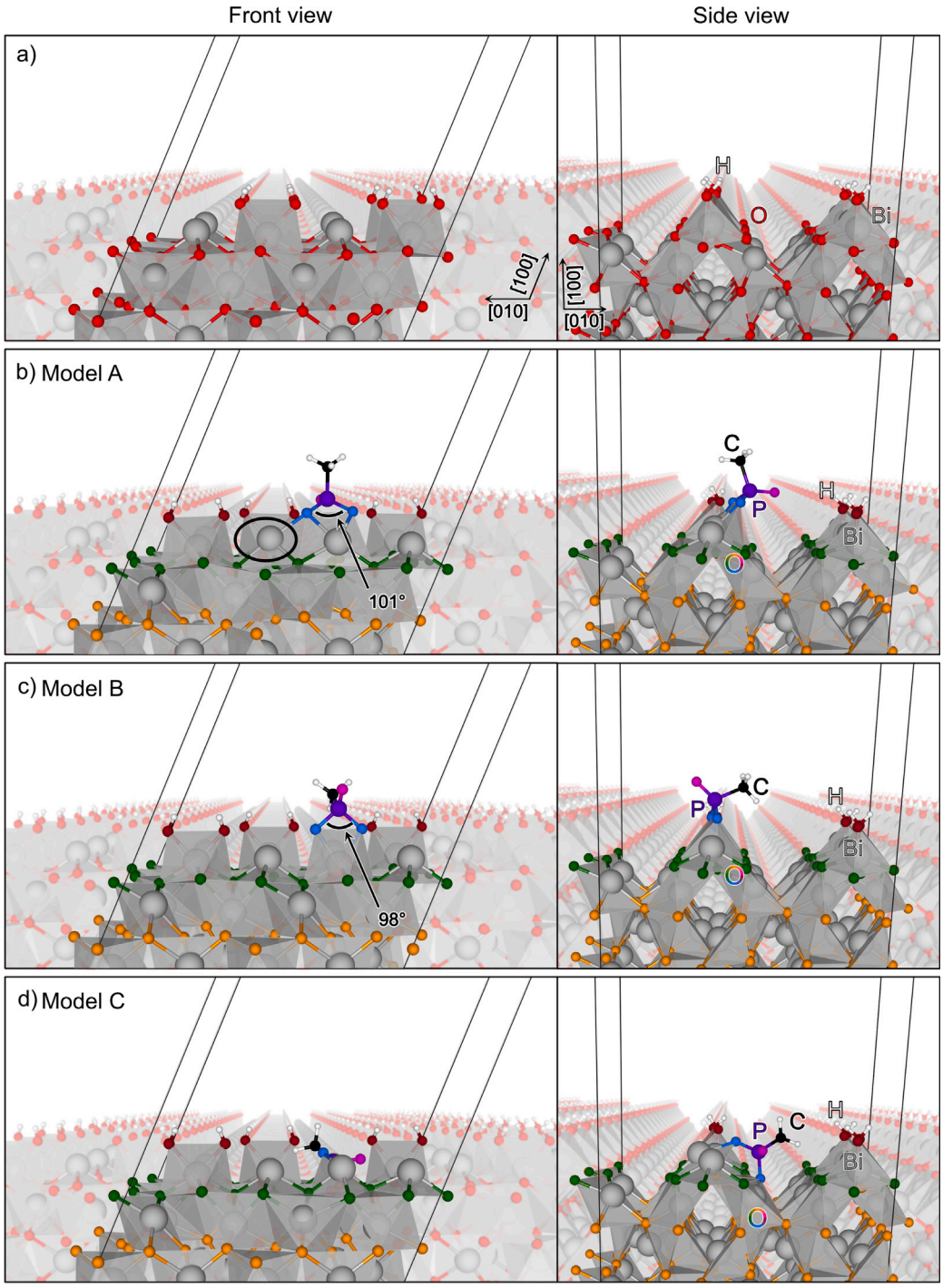

Fig. 3. (a) Structurally relaxed hydroxylated Bi_2O_3(100) surface. The hydroxyl groups have only a minor influence on the surface morphology, and form alternating chains of $BiO_4(OH)_2$-BiO_4 along the [001] direction. (b-d) Relaxed hydroxylated Bi_2O_3(100) surface with CH_3PO_3 adsorbed. Surface and bulk O atoms are represented by green and orange balls, respectively. The remaining O atoms are colored according to their coordination, more precisely, the ones in hydroxyl groups in burgundy, the P-coordinated one in magenta, and the P-Bi-coordinated O atoms in blue. Model A is by about 180 meV more favorable compared to model B. Model C obtained by allowing for O desorption from the surface is by about 1.5 eV less favorable than model A.

At this point, we would like to point out that the adsorption of phosphonic acids on the Bi_2O_3 surface could be accompanied by the desorption of O atoms from the surface, and there is also the possibility of adsorbed (or desorbed) H_2O molecules. To test this possibility, we replaced two of the OH groups as well as a O surface atom with the O atoms of the MPA molecule, also see model C in Fig. 3 (d). Nevertheless, we find that this configuration is by about 1.5 eV less favorable compared to model A and will thus not be considered further in this study.

4. XPS peak assignment

The experimental XPS survey data for the C 1*s*, O 1*s*, Bi 4*f*, and P 2*p* states of the bare and the ODPA-modified surface are shown in Fig. S5 in the Supplemental Material. Here, the O 1*s* spectra are fitted based on established models for experimental studies.

The compositions with respect to each element as determined from high-resolution spectra of each element are compiled in Table 2. The spectra indicate the presence of bismuth, oxygen and carbon on both

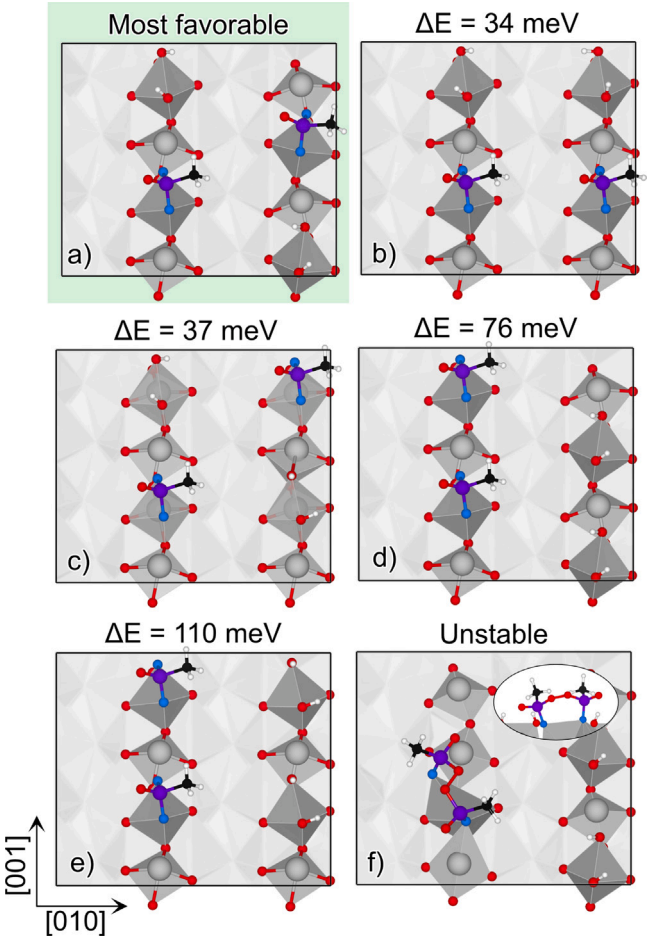

Fig. 4. Top view of the structurally relaxed hydroxylated Bi_2O_3(100) surface shown in Fig. 3 with two MPA molecules adsorbed at different relative positions. For clarity, the bulk O atoms are not shown and the O adatoms are colored in blue. The energies are given with respect to the most favorable structure. The structure (f), where the molecules adsorb on adjacent polyhedra, is not stable.

Table 2
Atomic composition of the bare and ODPA-modified Bi_2O_3 surface as measured by high-resolution XPS.

Substrate	C 1*s* (at.%)	O 1*s* (at.%)	Bi 4*f* (at.%)	P 2*p* (at.%)
Bi_2O_3	50.4	30.5	19.1	–
Bi_2O_3+ODPA	64.3	17.3	15.6	2.7

surfaces. The content of carbon for the pure bismuth oxide can be explained by typical contamination on the surface after exposure to the ambient atmosphere. Additionally, in the O 1*s* spectra interfacial water is detected. The O 1*s* peak of the pure Bi_2O_3 powder origins from both the Bi_2O_3 particles and oxygen-containing adsorbate layers such as carboxylates and an ice-like surface bound water layer. During the adsorption of ODPA such adsorbates are at least partially desorbed and substituted by the phosphonate molecule. Thereby, the O 1*s* signal decreases more strongly than the Bi 4*f* signal.

The O 1*s* XPS spectra are characteristic for the ODPA modification of the bismuth oxide surface. The experimental O 1*s* spectra for the bare Bi_2O_3, see gray curve in Fig. 5(a), clearly reveal a strong oxidic contribution at 530.2 eV, while the contribution at about 532.5 eV can be attributed to hydroxyl groups and/or interfacial water. The rather large peak widths can be explained by the defective surfaces of the particles as well as by the adsorption of carboxylic acids and water under ambient conditions. Water is indeed easily adsorbed on metal oxide surfaces based on hydrogen bonding [58]. Typically, one or two monolayers of ice-like structured water remain on oxide surfaces even at UHV conditions. Such layers can be detected, e.g., by temperature-controlled desorption (TPD) which shows that desorption of such layers occurs only at elevated temperatures (see, e.g., [58]). As the particle layer surface is not smooth but shows very rough topography, the actual take-off angle differs from the macroscopically adjusted angle. In addition, the adsorbate layer, consisting of a few water monolayers and surface-bound monolayers, is in the range of 1 to 3 nm thickness. Both effects contribute to the strong signature of the surface near region in the XPS spectra.

Upon adsorption of ODPA, the spectrum undergoes a noticeable transformation, see also gray curve in Fig. 5 (b) and (f). First of all, the comparison of the high-resolution XPS data shows a single peak for phosphorous. In addition, the contribution of adsorbed water decreases in intensity. This can be explained by the adsorption of the hydrophobic monolayer. Moreover, the oxidic contribution (BE = 529.5 eV) sharpens, while the hydroxylic component appears to be red-shifted by about 0.7 eV, and still seems to cover different surface states. This shift can be explained by the effect of charge neutralization, resulting in different full half widths (FHWM) for pristine and ODPA-modified Bi_2O_3. More precisely, the FHWM of ODPA-modified Bi_2O_3 is reduced to about 66.7% of the one for pristine Bi_2O_3, see also Fig. S5.

Due to the powder form, the resolution of the experimental XPS spectra is limited. For example, the O 1*s* peak of the phosphonate group (expected upon the ODPA modification at about 532.3 eV) cannot be clearly differentiated from the contributions tentatively attributed to the interfacial water and the hydroxyl groups. Thus, DFT simulations are carried out to assist in the interpretation of the XPS spectra, also see Fig. 5. To this end, we classify the O atoms in the systems according to their coordination number with respect of Bi, H, P and C. Then, we determine the binding energy of every O atom via the ΔSCF approach. The resulting energy distributions are smoothened using a 20 meV energy window and fitted with Gaussian-type functions. To account for the neutralization effect observed in the experiment (cf. Fig. S5), the FHWM of the Gaussian functions for the MPA-modified Bi_2O_3 surface was fixed to 66.7% of the one of the pristine surface. Finally, since the DFT binding energies can only be determined up to a common additive constant, a rigid shift of 740.92 eV and 740.20 eV for pristine and MPA-modified Bi_2O_3 surface, respectively, is applied in order to align the onset of the DFT spectra to the experimental ones.

For the bare surface, our DFT calculations confirm that the main peak in Fig. 5 (a) can be assigned to the surface (green) and bulk (orange) O atoms, while the secondary peak originates from the hydroxyl groups (burgundy). Nevertheless, since we do not account for interfacial water on the oxide surface, the secondary DFT peak is lower and more narrow compared to the experimental peak.

For the modified oxide, we simulate the XPS spectra for both models A and B discussed in Section 3.2. In fact, their total energies do not differ by more than 180 meV, and the exact geometry is sensitive to the monolayer density [41]. To understand the origin of the spectra of the ODPA-modified surface, we assign the contributions to the differently coordinated O species of the adsorption structure shown in Fig. 3 (b) and (c). Upon the phosphonic-acid absorption, two additional O types can be identified: One coordinated to both Bi and P, and one bonded to P, exclusively. These atoms give rise to additional peaks (light blue, and magenta, respectively). Notably, the relative position of the additional signals differs for the two models, cf. 5 (b) and (f). More precisely, for model A the additional signatures frame the peak attributed to surface O atoms. For model B, in contrast, they are located between the signatures of the hydroxyl group and the surface O atoms. So, our data suggest that these new oxygen types as well as the desorption of OH groups determine the XPS line shape.

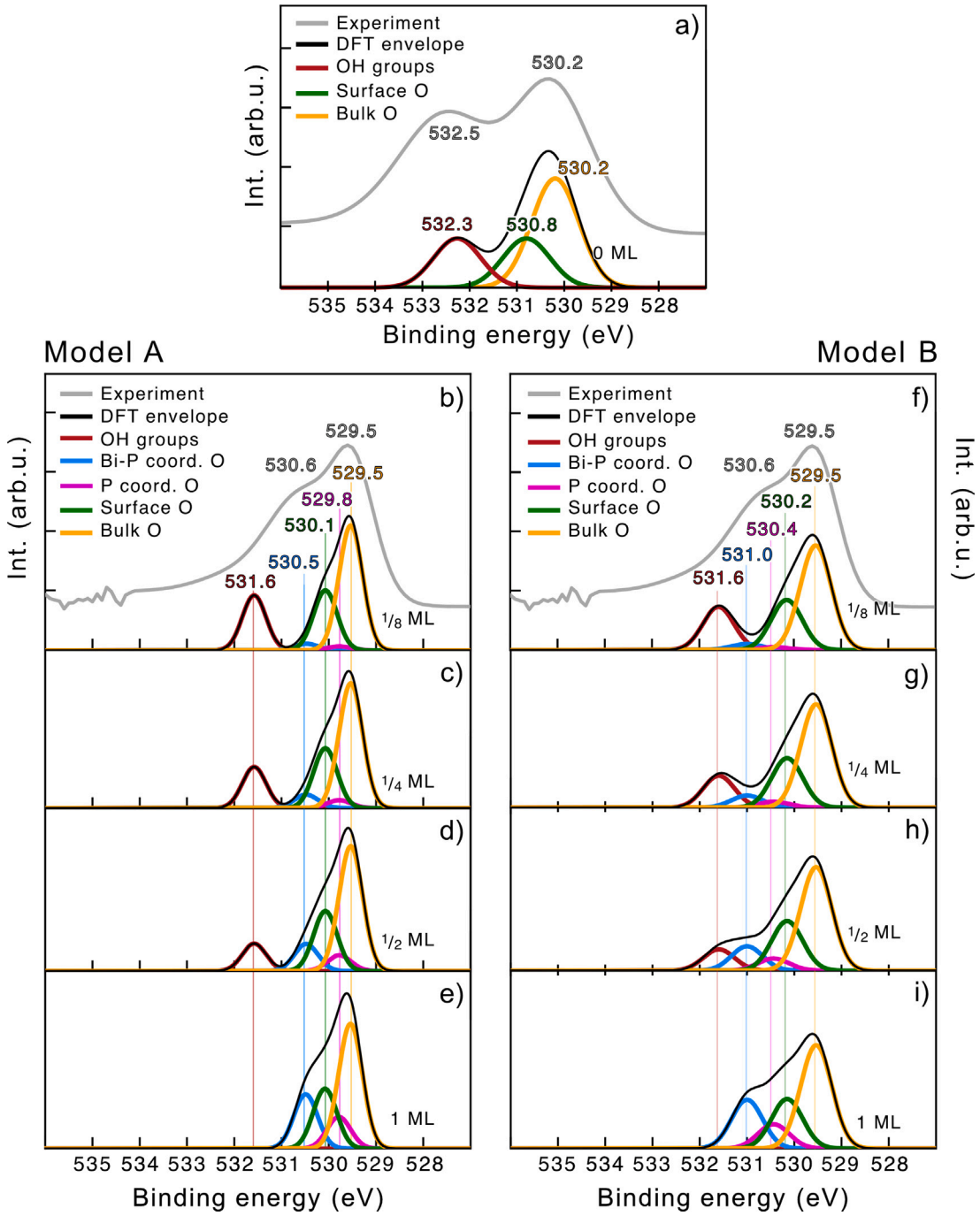

Fig. 5. Measured (gray) and simulated (black envelope) XPS data for O 1*s* on hydroxylated (a) and phosphonic acid adsorbed Bi_2O_3 surface for model A (b-e) and model B (f-i). The color coding used for the Gaussian fits corresponds to the colors used in Fig. 3 (b) and (c) for the different O types. Notably, both models A and B yield a good agreement with the experiment, suggesting the possibility of coexistence of both adsorbing geometries on modified BiO_2O_3 surfaces. Note that the experimental spectra correspond to the ones shown in Fig. S5 (b) in the Supplementary Material.

Nevertheless in both cases, the black envelope line of the DFT data does not fully reproduce the experimental spectrum. The former, in fact, still features a significant hydroxylic contribution, hinting that the DFT surface models deviate with respect of the monolayer density from the experimental system.

In order to simulate XPS spectra for higher phosphonic-acid coverages, we scale the intensities calculated for the models A and B shown in Fig. 3 b and c, respectively, to the respective stoichiometries for quarter, half, and full monolayer density, see Fig. 5 (c–e), and (g–i) for the two models A and B, respectively. This approximation is justified given that the core-level shifts are mainly determined by the local coordination and that the molecular adsorption leads to only minor structural relaxation of the surface. Notably, irrespective of the investigated DFT surface model, we find that the comparison of the simulated XPS spectra, i.e., the black envelope lines and experiment is best for full monolayer coverage. Notably, however, the experimental spectrum is broader and narrower compared to the DFT ones of the model A and model B, respectively. Thus, we suggest that both configurations can coexist on BiO_2O_3 surfaces. In addition, we note that in both cases the agreement with the experiment might be further improved by also

considering interfacial water in the DFT simulations. This is expected to give rise to additional signatures, contributing to the broader left shoulder of the experimental spectra.

5. Summary and conclusions

The adsorption of octadecylphosphonic acid on α-Bi_2O_3 surfaces was investigated with XPS and DRIFTS. The resulting data were analyzed with the help of DFT total-energy calculations and theoretical spectroscopy for a model system, methylphosphonic acid adsorbed on the α-Bi_2O_3(100) surface. Our results show that a full mononolayer of phosphonic acid forms, with an all-trans configuration of the aliphatic chains. Thereby, the phosphonates are expected to predominantly assume a bidentate configuration. The XPS signatures can be utilized to control the monolayer coverage, and therefore the adsorption mechanisms. It can be concluded that organophosphonic acids can be successfully used to functionalize and protect Bi_2O_3 covered Bi electrodes from oxidation.

CRediT authorship contribution statement

A. Bocchini: Writing – original draft, Visualization, Software, Methodology, Investigation, Formal analysis, Data curation. **S. Kollmann:** Writing – original draft, Visualization, Methodology, Investigation, Formal analysis, Data curation. **U. Gerstmann:** Writing – review & editing, Software, Methodology, Funding acquisition. **W.G. Schmidt:** Writing – review & editing, Methodology, Funding acquisition, Conceptualization. **G. Grundmeier:** Writing – review & editing, Methodology, Conceptualization.

Declaration of competing interest

The authors declare the following financial interests/personal relationships which may be considered as potential competing interests: Adriana Bocchini reports financial support was provided by German Research Foundation. Uwe Gerstmann reports financial support was provided by German Research Foundation. Wolf Gero Schmidt reports financial support was provided by German Research Foundation. If there are other authors, they declare that they have no known competing financial interests or personal relationships that could have appeared to influence the work reported in this paper.

Acknowledgments

The DFG, Germany (TRR 142/3-2025 – Project No. 231447078) is gratefully acknowledged for financial support. We thank the Paderborn Center for Parallel Computing (PC^2) and the Höchstleistungs-Rechenzentrum Stuttgart (HLRS) for grants of high-performance computer time. Furthermore, we thank Tobias Wagner (Department of Inorganic Chemistry, Paderborn University, Paderborn, Germany) for XRD measurement.

Appendix A. Supplementary data

Supplementary material related to this article can be found online at https://doi.org/10.1016/j.susc.2025.122776.

Data availability

Data will be made available on request.

References

[1] M.A. Ud Din, C. Li, L. Zhang, C. Han, B. Li, Recent progress and challenges on the bismuth-based anode for sodium-ion batteries and potassium-ion batteries, Mater. Today Phys. 21 (2021) 100486, http://dx.doi.org/10.1016/j.mtphys.2021.100486, URL: https://www.sciencedirect.com/science/article/pii/S2542529321001474.

[2] A. Wijesekara, Y. Han, D. Walker, S. Huband, R. Hatton, Highly air stable tin halide perovskite photovoltaics using a bismuth capped copper top electrode, Adv. Sci. 10 (2023) 2301497, http://dx.doi.org/10.1002/advs.202301497, arXiv: https://onlinelibrary.wiley.com/doi/pdf/10.1002/advs.202301497.

[3] B.H. Yun, K.J. Kim, D.W. Joh, M.S. Chae, J.J. Lee, D.w. Kim, S. Kang, D. Choi, S.T. Hong, K.T. Lee, Highly active and durable double-doped bismuth oxide-based oxygen electrodes for reversible solid oxide cells at reduced temperatures, J. Mater. Chem. A 7 (2019) 20558–20566, http://dx.doi.org/10.1039/C9TA09203J.

[4] D.H. Nam, K.S. Choi, Bismuth as a new chloride-storage electrode enabling the construction of a practical high capacity desalination battery, J. Am. Chem. Soc. 139 (2017) 11055–11063, http://dx.doi.org/10.1021/jacs.7b01119, pMID: 28777553.

[5] J. Zeng, N.B. Monti, T. Chen, M. Castellino, W. Ju, M.A. Louren¸co, P. Jagdale, C.F. Pirri, Evolution of bismuth electrodes activating electrosynthesis of formate from carbon dioxide reduction, Catal. Today 437 (2024) 114743, http://dx.doi.org/10.1016/j.cattod.2024.114743, URL: https://www.sciencedirect.com/science/article/pii/S0920586124002372.

[6] Y. Wang, X. Zhu, Y. Li, Spin–orbit coupling-dominated catalytic activity of two-dimensional bismuth toward co2 electroreduction: Not the thinner the better, J. Phys. Chem. Lett. 10 (2019) 4663–4667, http://dx.doi.org/10.1021/acs.jpclett.9b01406, pMID: 31314533.

[7] V. Jovanovski, S.B. Hočevar, B. Ogorevc, Bismuth electrodes in contemporary electroanalysis, Curr. Opin. Electrochem. 3 (2017a) 114–122, http://dx.doi.org/10.1016/j.coelec.2017.07.008, URL: https://www.sciencedirect.com/science/article/pii/S2451910317300352.

[8] C. Gu, S. Zhu, Z. Gu, Advances in bismuth utilization for biomedical applications – from a bibliometric perspective, Coord. Chem. Rev. 517 (2024) 215988, http://dx.doi.org/10.1016/j.ccr.2024.215988, URL: https://www.sciencedirect.com/science/article/pii/S0010854524003345.

[9] C. Zhang, C. Li, X. Han, Screen printed electrode containing bismuth for the detection of cadmium ion, J. Electroanal. Chem. 933 (2023) 117291, http://dx.doi.org/10.1016/j.jelechem.2023.117291, URL: https://www.sciencedirect.com/science/article/pii/S1572665723001510.

[10] Z. Dang, W. Wang, J. Chen, E.S. Walker, S.R. Bank, D. Akinwande, Z. Ni, L. Tao, Vis-nir photodetector with microsecond response enabled by 2d bismuth/si(111) heterojunction, 2D Mater. 8 (2021) 035002, http://dx.doi.org/10.1088/2053-1583/abea65.

[11] X.J. Dai, X.X. Niu, W.Q. Fu, D. Zheng, W.X. Liu, W.H. Shi, J.W. Nai, F.F. Wu, X.H. Cao, Bismuth-based materials for rechargeable aqueous batteries and water desalination, Rare Met. 41 (2022) 287–303, http://dx.doi.org/10.1007/s12598-021-01853-7.

[12] Y. Jiang, S.I. Alhassan, D. Wei, H. Wang, A review of battery materials as cdi electrodes for desalination, Water 12 (2020) 3030, http://dx.doi.org/10.3390/w12113030, URL: https://www.mdpi.com/2073-4441/12/11/3030.

[13] V. Jovanovski, S.B. Hočevar, B. Ogorevc, Bismuth electrodes in contemporary electroanalysis, Curr. Opin. Electrochem. 3 (2017b) 114–122, http://dx.doi.org/10.1016/j.coelec.2017.07.008, URL: https://www.sciencedirect.com/science/article/pii/S2451910317300352.

[14] J. Wang, Stripping analysis at bismuth electrodes: A review, Electroanalysis 17 (2005) 1341–1346, http://dx.doi.org/10.1002/elan.200403270.

[15] L.O.S. Colbin, T.E. Nwafornso, Y. Li, R. Younesi, On the compatibility of high mass loading bismuth anodes for full-cell sodium-ion batteries, Dalton Trans. 51 (2022) 16852–16860, http://dx.doi.org/10.1039/D2DT02686D, URL: http://dx.doi.org/10.1039/D2DT02686D.

[16] C. König, J.C. Greer, S. Fahy, Electronic properties of bismuth nanostructures, Phys. Rev. B 104 (2021) 045432, http://dx.doi.org/10.1103/PhysRevB.104.045432, URL: https://link.aps.org/doi/10.1103/PhysRevB.104.045432.

[17] W. Oh, C.K. Rhee, J.W. Han, B. Shong, Atomic and molecular adsorption on the bi(111) surface: Insights into catalytic co2 reduction, J. Phys. Chem. C 122 (2018) 23084–23090, http://dx.doi.org/10.1021/acs.jpcc.8b07865.

[18] E. Puckrin, A.J. Slavin, Adsorption of bismuth onto the au(111) surface, Phys. Rev. B 41 (1990) 4970–4975, http://dx.doi.org/10.1103/PhysRevB.41.4970, URL: https://link.aps.org/doi/10.1103/PhysRevB.41.4970.

[19] L. Leontie, M. Caraman, M. Alexe, C. Harnagea, Structural and optical characteristics of bismuth oxide thin films, Surf. Sci. 507–510 (2002) 480–485, http://dx.doi.org/10.1016/S0039-6028(02)01289-X, URL: https://www.sciencedirect.com/science/article/pii/S003960280201289X.

[20] L. Leontie, M. Caraman, A. Visinoiu, G. Rusu, On the optical properties of bismuth oxide thin films prepared by pulsed laser deposition, Thin Solid Films 473 (2005) 230–235, http://dx.doi.org/10.1016/j.tsf.2004.07.061, URL: https://www.sciencedirect.com/science/article/pii/S0040609004010041.

[21] S.Z. Hao, D. Zhou, L.X. Pang, M.Z. Dang, S.K. Sun, T. Zhou, S. Trukhanov, A. Trukhanov, A.S.B. Sombra, Q. Li, X.Q. Zhang, S. Xia, M.A. Darwish, Ultra-low temperature co-fired ceramics with adjustable microwave dielectric properties in the na2o–bi2o3–moo3 ternary system: a comprehensive study, J. Mater. Chem. C 10 (2022) 2008–2016, http://dx.doi.org/10.1039/D1TC05557G.

[22] M. Jacob, H. Nguyen, M. Neurock, A. Bhan, Kinetics of redox half-cycles on bi2o3 for the selective catalytic combustion of hydrogen, ACS Catal. 14 (2024) 4568–4580, http://dx.doi.org/10.1021/acscatal.3c05585.

[23] H. Cheng, B. Huang, J. Lu, Z. Wang, B. Xu, X. Qin, X. Zhang, Y. Dai, Synergistic effect of crystal and electronic structures on the visible-light-driven photocatalytic performances of Bi_2O_3 polymorphs, Phys. Chem. Chem. Phys. 12 (2010) 15468–15475, http://dx.doi.org/10.1039/C0CP01189D.

[24] G.Alessio. Verni, B. Long, F. Gity, M. Lanius, P. Schüffelgen, G. Mussler, D. Grützmacher, J. Greer, J.D. Holmes, Oxide removal and stabilization of bismuth thin films through chemically bound thiol layers, RSC Adv. 8 (2018) 33368–33373, http://dx.doi.org/10.1039/C8RA06840B.

[25] J.C. Love, L.A. Estroff, J.K. Kriebel, R.G. Nuzzo, G.M. Whitesides, Self-assembled monolayers of thiolates on metals as a form of nanotechnology, Chem. Rev. 105 (2005) 1103–1170, http://dx.doi.org/10.1021/cr0300789, pMID: 15826011.

[26] M. Adamovski, A. Zajac, P. Gründler, G.U. Flechsig, Self-assembled monolayers on bismuth electrodes, Electrochem. Commun. 8 (2006) 932–936, http://dx.doi.org/10.1016/j.elecom.2006.03.031, URL: https://www.sciencedirect.com/science/article/pii/S1388248106001305.

[27] A. Cattani-Scholz, Functional organophosphonate interfaces for nanotechnology: A review, ACS Appl. Mater. & Interfaces 9 (2017) 25643–25655, http://dx.doi.org/10.1021/acsami.7b04382, pMID: 28671811.

[28] T. Hauffman, L. Van Lokeren, R. Willem, A. Hubin, H. Terryn, In situ study of the deposition of (ultra)thin organic phosphonic acid layers on the oxide of aluminum, Langmuir 28 (2012) 3167–3173, http://dx.doi.org/10.1021/la203988m, pMID: 22242677.

[29] R. Zhao, P. Schmutz, L.P.H. Jeurgens, J. Chen, A. Gooneie, N. Ott, S. Gaan, M. Heuberger, Two steady-state adsorption modes of phosphonic acids on aluminum surfaces, ACS Appl. Mater. & Interfaces 14 (2022) 39467–39477, http://dx.doi.org/10.1021/acsami.2c07128, pMID: 35994435.

[30] M. Maxisch, C. Ebbert, B. Torun, N. Fink, T. de los Arcos, J. Lackmann, H. Maier, G. Grundmeier, Pm-irras studies of the adsorption and stability of organophosphonate monolayers on passivated niti surfaces, Appl. Surf. Sci. 257 (2011a) 2011–2018, http://dx.doi.org/10.1016/j.apsusc.2010.09.044, URL: https://www.sciencedirect.com/science/article/pii/S0169433210012766.

[31] M. Alexander, G. Beamson, C. Blomfield, G. Leggett, T. Duc, Interaction of carboxylic acids with the oxyhydroxide surface of aluminium: poly(acrylic acid), acetic acid and propionic acid on pseudoboehmite, J. Electron Spectrosc. Relat. Phenom. 121 (2001) 19–32, http://dx.doi.org/10.1016/S0368-2048(01)00324-3, URL: https://www.sciencedirect.com/science/article/pii/S0368204801003243, electron Spectroscopy of polymer surfaces.

[32] C. Kunze, M. Valtiner, R. Michels, K. Huber, G. Grundmeier, Self-localization of polyacrylic acid molecules on polar zno(0001)–zn surfaces, Phys. Chem. Chem. Phys 13 (2011) 12959–12967, http://dx.doi.org/10.1039/C1CP20913B, URL: http://dx.doi.org/10.1039/C1CP20913B.

[33] I.L. Liakos, R.C. Newman, E. McAlpine, M.R. Alexander, Comparative study of self-assembly of a range of monofunctional aliphatic molecules on magnetron-sputtered aluminium, Surf. Interface Anal. 36 (2004) 347–354, http://dx.doi.org/10.1002/sia.1749.

[34] P. Thissen, J. Wielant, M. Köyer, S. Toews, G. Grundmeier, Formation and stability of organophosphonic acid monolayers on znal alloy coatings, Surf. Coat. Technol. 204 (2010a) 3578–3584, http://dx.doi.org/10.1016/j.surfcoat.2010.04.027, URL: https://www.sciencedirect.com/science/article/pii/S025789721000294X.

[35] J.van.den. Brand, O. Blajiev, P.C.J. Beentjes, H. Terryn, J.H.W. de Wit, Interaction of anhydride and carboxylic acid compounds with aluminum oxide surfaces studied using infrared reflection absorption spectroscopy, Langmuir 20 (2004) 6308–6317, http://dx.doi.org/10.1021/la0496845, pMID: 15248717.

[36] N. Tillman, A. Ulman, J.S. Schildkraut, T.L. Penner, Incorporation of phenoxy groups in self-assembled monolayers of trichlorosilane derivatives, effects on film thickness, wettability, and molecular orientation, J. Am. Chem. Soc. 110 (1988) 6136–6144.

[37] C. Bram, C. Jung, M. Stratmann, Self assembled molecular monolayers on oxidized inhomogeneous aluminum surfaces, Fresenius' J. Anal. Chem. 358 (1997) 108–111, http://dx.doi.org/10.1007/s002160050357.

[38] R. Boissezon, J. Muller, V. Beaugeard, S. Monge, J.J. Robin, Organophosphonates as anchoring agents onto metal oxide-based materials: synthesis and applications, RSC Adv. 4 (2014) 35690–35707, http://dx.doi.org/10.1039/C4RA05414H, URL: http://dx.doi.org/10.1039/C4RA05414H.

[39] P. Thissen, M. Valtiner, G. Grundmeier, Stability of phosphonic acid self-assembled monolayers on amorphous and single-crystalline aluminum oxide surfaces in aqueous solution, Langmuir 26 (2010b) 156–164, http://dx.doi.org/10.1021/la900935s, pMID: 20000361.

[40] P. Thissen, A. Vega, T. Peixoto, Y.J. Chabal, Controlled, low-coverage metal oxide activation of silicon for organic functionalization: unraveling the phosphonate bond, Langmuir 28 (2012) 17494–17505, http://dx.doi.org/10.1021/la3038457, pMID: 23163566.

[41] C. Schuschke, M. Schwarz, C. Hohner, T.N. Silva, L. Fromm, T. Döpper, A. Görling, J. Libuda, Phosphonic acids on an atomically defined oxide surface: The binding motif changes with surface coverage, J. Phys. Chem. Lett. 9 (2018) 1937–1943, http://dx.doi.org/10.1021/acs.jpclett.8b00668, pMID: 29595985.

[42] P. Giannozzi, S. Baroni, N. Bonini, M. Calandra, R. Car, C. Cavazzoni, D. Ceresoli, G.L. Chiarotti, M. Cococcioni, I. Dabo, A.D. Corso, S.de. Gironcoli, S. Fabris, G. Fratesi, R. Gebauer, U. Gerstmann, C. Gougoussis, A. Kokalj, M. Lazzeri, L. Martin-Samos, N. Marzari, F. Mauri, R. Mazzarello, S. Paolini, A. Pasquarello, L. Paulatto, C. Sbraccia, S. Scandolo, G. Sclauzero, A.P. Seitsonen, A. Smogunov, P. Umari, R.M. Wentzcovitch, Quantum espresso: a modular and open-source software project for quantum simulations of materials, J. Phys.: Condens. Matter. 21 (2009) 395502, http://dx.doi.org/10.1088/0953-8984/21/39/395502, URL: https://iopscience.iop.org/article/10.1088/0953-8984/21/39/395502.

[43] P. Giannozzi, O. Andreussi, T. Brumme, O. Bunau, M.B. Nardelli, M. Calandra, R. Car, C. Cavazzoni, D. Ceresoli, M. Cococcioni, N. Colonna, I. Carnimeo, A.D. Corso, S.de. Gironcoli, P. Delugas, R.A. DiStasio, A. Ferretti, A. Floris, G. Fratesi, G. Fugallo, R. Gebauer, U. Gerstmann, F. Giustino, T. Gorni, J. Jia, M. Kawamura, H.Y. Ko, A. Kokalj, E. Küçükbenli, M. Lazzeri, M. Marsili, N. Marzari, F. Mauri, N.L. Nguyen, H.V. Nguyen, A.O. de-la Roza, L. Paulatto, S. Poncé, D. Rocca, R. Sabatini, B. Santra, M. Schlipf, A.P. Seitsonen, A. Smogunov, I. Timrov, T. Thonhauser, P. Umari, N. Vast, X. Wu, S. Baroni, Advanced capabilities for materials modelling with quantum ESPRESSO, J. Phys.: Condens. Matter. 29 (2017) 465901, http://dx.doi.org/10.1088/1361-648x/aa8f79, URL: https://iopscience.iop.org/article/10.1088/1361-648X/aa8f79.

[44] J.P. Perdew, K. Burke, M. Ernzerhof, Generalized gradient approximation made simple, Phys. Rev. Lett. 77 (1996) 3865–3868, http://dx.doi.org/10.1103/PhysRevLett.77.3865.

[45] G. Malmros, The crystal structure of alpha-bi_2o_3, Acta Chem. Scand. 24 (1970) 384, URL: http://actachemscand.org/pdf/acta_vol_24_p0384-0396.pdf.

[46] J.E. Saal, S. Kirklin, M. Aykol, B. Meredig, C. Wolverton, Materials design and discovery with high-throughput density functional theory: The open quantum materials database (oqmd), JOM 65 (2013) 1501, http://dx.doi.org/10.1007/s11837-013-0755-4.

[47] S. Kirklin, J.E. Saal, B. Meredig, A. Thompson, J.W. Doak, M. Aykol, S. Rühl, C. Wolverton, The open quantum materials database (oqmd): assessing the accuracy of dft formation energies, Npj Comput. Mater. 1 (2015) 15010, http://dx.doi.org/10.1038/npjcompumats.2015.10.

[48] Y.H. Lei, Z.X. Chen, Density functional study of the stability of various α-Bi_2O_3 surfaces, J. Chem. Phys. 138 (2013) 054703, http://dx.doi.org/10.1063/1.4788667, arXiv:https://pubs.aip.org/aip/jcp/article-pdf/doi/10.1063/1.4788667/13311570/054703_1_online.pdf.

[49] H.J. Monkhorst, J.D. Pack, Special points for brillouin-zone integrations, Phys. Rev. B 13 (1976) 5188–5192, http://dx.doi.org/10.1103/PhysRevB.13.5188.

[50] E. Pehlke, M. Scheffler, Evidence for site-sensitive screening of core holes at the si and ge (001) surface, Phys. Rev. Lett. 71 (1993) 2338–2341, http://dx.doi.org/10.1103/PhysRevLett.71.2338.

[51] P. Käckell, W.G. Schmidt, F. Bechstedt, Se-induced 3d core-level shifts of gaas(110), Appl. Surf. Sci. 104–105 (1996) 141–146, http://dx.doi.org/10.1016/S0169-4332(96)00135-3, URL: https://www.sciencedirect.com/science/article/pii/S0169433296001353.

[52] W.G. Schmidt, P. Käckell, F. Bechstedt, 3D core-level shifts at segaas(110), Surf. Sci. 357–358 (1996) 545–549, http://dx.doi.org/10.1016/0039-6028(96)00220-8, URL: https://www.sciencedirect.com/science/article/pii/0039602896002208.

[53] S. Garcia-Gil, A. Garcia, P. Ordejon, Calculation of core level shifts within dft using pseudopotentials and localized basis sets, Eur. Phys. J. B 85 (2012) 239, http://dx.doi.org/10.1140/epjb/e2012-30334-5.

[54] M. Franz, S. Chandola, M. Koy, R. Zielinski, H. Aldahhak, M. Das, M. Freitag, U. Gerstmann, D. Liebig, A.K. Hoffmann, M. Rosin, W.G. Schmidt, C. Hogan, F. Glorius, N. Esser, M. Dähne, Controlled growth of ordered monolayers of n-heterocyclic carbenes on silicon, Nat. Chem. 13 (2021) 828, http://dx.doi.org/10.1038/s41557-021-00721-2.

[55] D.M. Spori, N.V. Venkataraman, S.G.P. Tosatti, F. Durmaz, N.D. Spencer, S. Zürcher, Influence of alkyl chain length on phosphate self-assembled monolayers, Langmuir 23 (2007) 8053–8060, http://dx.doi.org/10.1021/la700474v, pMID: 17569549.

[56] M. Maxisch, P. Thissen, M. Giza, G. Grundmeier, Interface chemistry and molecular interactions of phosphonic acid self-assembled monolayers on oxyhydroxide-covered aluminum in humid environments, Langmuir 27 (2011b) 6042–6048, http://dx.doi.org/10.1021/la200445x, pMID: 21488681.

[57] K. Pohl, J. Otte, P. Thissen, M. Giza, M. Maxisch, B. Schuhmacher, G. Grundmeier, Adsorption and stability of self-assembled organophosphonic acid monolayers on plasma modified zn–mg–al alloy surfaces, Surf. Coat. Technol. 218 (2013) 99–107, http://dx.doi.org/10.1016/j.surfcoat.2012.12.035, URL: https://www.sciencedirect.com/science/article/pii/S0257897212012819.

[58] M. Egashira, M. Nakashima, S. Kawasumi, T. Selyama, Temperature programmed desorption study of water adsorbed on metal oxides. 2. tin oxide surfaces, J. Phys. Chem. 85 (1981) 4125–4130.